



**Proton Donor Acidity Controls Selectivity in Nonaromatic Nitrogen Heterocycle Synthesis**

Simon Duttwyler *et al.*  
*Science* **339**, 678 (2013);  
DOI: 10.1126/science.1230704

---

*This copy is for your personal, non-commercial use only.*

---

**If you wish to distribute this article to others**, you can order high-quality copies for your colleagues, clients, or customers by [clicking here](#).

**Permission to republish or repurpose articles or portions of articles** can be obtained by following the guidelines [here](#).

**The following resources related to this article are available online at [www.sciencemag.org](http://www.sciencemag.org) (this information is current as of February 18, 2013 ):**

**Updated information and services**, including high-resolution figures, can be found in the online version of this article at:

<http://www.sciencemag.org/content/339/6120/678.full.html>

**Supporting Online Material** can be found at:

<http://www.sciencemag.org/content/suppl/2013/02/07/339.6120.678.DC1.html>

This article appears in the following **subject collections**:

Chemistry

<http://www.sciencemag.org/cgi/collection/chemistry>

Although local flexural stresses or structural control can alter the orientations of intrusions (7), the LGAs are distributed uniformly across the Moon and show no clear preferred orientations or association with known flexurally supported loads. This pattern indicates largely isotropic horizontal extension, as would be expected to arise from global expansion. However, the lunar lithosphere is thought to have been in a state of compression throughout most of its history as a result of interior cooling and global contraction (28). Superimposed stresses associated with the outward migration of the Moon, with or without contemporaneous true polar wander, are similarly inconsistent with the locations and orientations of the LGAs (7, 29). At the time of the intrusive activity inferred here, the lithosphere must have been in a horizontally extensional stress state to accommodate the inflation of the vertical tabular intrusions. Taking the total length of the probable intrusion population of 5300 km and the typical best-fit widths of 5 to 40 km, the resulting horizontal extensional strain of 0.035 to 0.27% equates to an increase in the lunar radius by 0.6 to 4.8 km. However, this estimate is complicated by the possibility of viscous accommodation of some of the growth of the intrusions or lithospheric extension not accompanied by intrusive activity that would go undetected by GRAIL.

Such a period of early extension was predicted by some thermal history models (28), developed to account for the absence of a global population of large thrust faults on the Moon similar to those found on Mercury. The thermal models best matched that constraint with an initial condition that included a 200- to 300-km-deep magma ocean and a cooler deep interior, leading to coupled warming of the interior and cooling of the outer shell, with net expansion in the first billion years followed by modest global contraction. Cooling and contraction of the lunar lithosphere could also have contributed to extensional strain at the depths of these intrusions within the first few tens of millions of years after lunar crustal formation. This thermal inversion may be a natural outcome of the post-accretional temperature profile of the Moon (30). Thermal history models that satisfy the constraint of <1 km decrease in radius over the past 3.8 billion years (Gy) also predict 2.7 to 3.7 km of global expansion during the first ~1 Gy, with the highest rates occurring during the first 0.5 Gy (28), consistent with our proposed period of expansion. The amount of predicted expansion is sensitive to the depth of the magma ocean and the initial temperature of the deep interior. However, no direct geological evidence for this early expansion has previously been found, as a consequence of the intense cratering of the surface at that time. This earliest epoch of lunar expansion is now revealed by GRAIL gravity data, which allows us to see through the surface geology to the hidden structures beneath. This result places a constraint on lunar evolution and raises important questions regarding the early evolution of other terrestrial

planets, because the first ~700 My of planetary evolution is poorly preserved in the geological records of all planets.

#### References and Notes

- W. K. Hartmann, R. W. Gaskell, *Meteoritics* **32**, 109 (1997).
- D. Stöffler, G. Ryder, *Space Sci. Rev.* **96**, 9 (2001).
- M. T. Zuber *et al.*, *Space Sci. Rev.* 10.1007/s11214-012-9952-7 (2013).
- M. T. Zuber *et al.*, *Science* **339**, 668 (2013).
- C. Jekeli, *Surv. Geophys.* **27**, 257 (2006).
- R. Rummel, W. Yi, C. Stummer, *J. Geod.* **85**, 777 (2011).
- Materials and methods are available as supplementary materials on Science Online.
- M. A. Wieczorek *et al.*, *Science* **339**, 671 (2013).
- W. S. Kiefer, R. J. Macke, D. T. Britt, A. J. Irving, G. J. Consolmagno, *Geophys. Res. Lett.* **39**, L07201 (2012).
- R. E. Ernst, E. B. Grosfils, D. Mège, *Annu. Rev. Earth Planet. Sci.* **29**, 489 (2001).
- L. Wilson, J. W. Head III, *Lunar Planet. Sci.* **40**, abstract 1160 (2009).
- A. M. Rubin, *Earth Planet. Sci. Lett.* **119**, 641 (1993).
- A. H. Wilson, *J. Petrol.* **23**, 240 (1982).
- F. Podmore, A. H. Wilson, "A reappraisal of the structure and emplacement of the Great Dyke, Zimbabwe," *Geol. Assoc. Canada Special Paper 33* (1985), pp. 317–330.
- D. Mège, A. C. Cook, E. Garel, Y. Lagabrielle, M. Cormier, *J. Geophys. Res.* **108**, 5044 (2003).
- J. C. Andrews-Hanna, *J. Geophys. Res.* **117**, E04009 (2012).
- M. E. Purucker, J. W. Head III, L. Wilson, *J. Geophys. Res.* **117**, E05001 (2012).
- A. Gudmundsson, *J. Volcanol. Geotherm. Res.* **64**, 1 (1995).
- J. W. Head III, L. Wilson, *Geophys. Res. Lett.* **18**, 2121 (1991).
- J. W. Head III, L. Wilson, *Planet. Space Sci.* **41**, 719 (1993).
- M. A. Wieczorek, B. P. Weiss, S. T. Stewart, *Science* **335**, 1212 (2012).
- M. E. Purucker, J. B. Nicholas, *J. Geophys. Res.* **115**, E12007 (2010).
- D. E. Smith *et al.*, *Geophys. Res. Lett.* **37**, L18204 (2010).
- A. M. Rubin, *J. Geophys. Res.* **97**, 1839 (1992).
- J. C. Andrews-Hanna, *Icarus* **222**, 159 (2013).
- G. A. Snyder, C. R. Neal, L. A. Taylor, A. N. Halliday, *J. Geophys. Res.* **100**, 9365 (1995).
- E. M. Anderson, *The Dynamics of Faulting and Dyke Formation with Application to Britain* (Oliver and Boyd, London, ed. 2, 1951).
- S. C. Solomon, *Phys. Earth Planet. Inter.* **15**, 135 (1977).
- H. J. Melosh, *Icarus* **43**, 334 (1980).
- W. M. Kaula, *J. Geophys. Res.* **84**, 999 (1979).

**Acknowledgments:** The GRAIL mission is a component of the NASA Discovery Program and is performed under contract to the Massachusetts Institute of Technology and the Jet Propulsion Laboratory. J.C.A.-H., J.W.H., W.S.K., I.M., P.J.M., F.N., and G.J.T. were supported by grants from the NASA GRAIL Guest Scientist Program. The data used in this study will have been archived in the Geosciences Node of the NASA Planetary Data System by the time of publication.

#### Supplementary Materials

www.sciencemag.org/cgi/content/full/science.1231753/DC1  
Materials and Methods  
Supplementary Text  
Figs. S1 to S13  
Tables S1 to S6  
References (31–47)

19 October 2012; accepted 27 November 2012  
Published online 5 December 2012;  
10.1126/science.1231753

## Proton Donor Acidity Controls Selectivity in Nonaromatic Nitrogen Heterocycle Synthesis

Simon Duttwyler,<sup>1</sup> Shuming Chen,<sup>1</sup> Michael K. Takase,<sup>1</sup> Kenneth B. Wiberg,<sup>1</sup> Robert G. Bergman,<sup>2</sup> Jonathan A. Ellman<sup>1\*</sup>

Piperidines are prevalent in natural products and pharmaceutical agents and are important synthetic targets for drug discovery and development. We report on a methodology that provides highly substituted piperidine derivatives with regiochemistry selectively tunable by varying the strength of acid used in the reaction. Readily available starting materials are first converted to dihydropyridines via a cascade reaction initiated by rhodium-catalyzed carbon-hydrogen bond activation. Subsequent divergent regio- and diastereoselective protonation of the dihydropyridines under either kinetic or thermodynamic control provides two distinct iminium ion intermediates that then undergo highly diastereoselective nucleophilic additions. X-ray structural characterization of both the kinetically and thermodynamically favored iminium ions along with density functional theory calculations provide a theoretical underpinning for the high selectivities achieved for the reaction sequences.

**P**iperidines are saturated, nonplanar nitrogen heterocycles upon which the display of functionality has provided some of the most well-known pharmaceuticals, as exemplified by traditional drugs such as quinine, morphine (and its many synthetic analogs such as oxycodone), as well as a number of more recent blockbuster drugs, including plavix for the treat-

ment of stroke, cialis for erectile dysfunction, and aricept for Alzheimer's treatment (Fig. 1A) (1). The physical properties and therapeutic importance of the piperidine scaffold are consistent with recent retrospective analyses of drug-discovery research suggesting that renewed emphasis should be placed on the preparation, evaluation, and development of compounds with

increased saturation and nonplanar display of functionality (2–4).

C–H bond functionalization has emerged as a powerful approach for the synthesis and modification of planar, aromatic *N*-heterocycles from cheap and readily available precursors (5–11). Recently, we reported on a cascade reaction comprising rhodium-catalyzed C–H activation of imines **1** with coupling to alkynes **2** to give azatrienes **3** followed by electrocyclization to provide densely substituted 1,2-dihydropyridines **4** (Fig. 1B) (12–15). These relatively unstable nonaromatic *N*-heterocycles can readily be aromatized to stable pyridines. Dihydropyridines **4** can also be converted to more highly saturated heterocycles (16); however, densely substituted derivatives have previously been difficult to access and pose a particular challenge in terms of regio- and stereochemical transformation. Recently, we demonstrated an in situ protonation/reduction sequence that provides tetrahydropyridines **7** with very high regio- and diastereoselectivity (17). Here, we demonstrate that tetrahydropyridines **8** with an alternative substitution pattern and stereochemical display can be accessed by tuning the strength of the acid used. In addition to

hydride, a range of carbon nucleophiles have also been added to both iminium intermediates **5** and **6** to provide even more densely substituted derivatives of **7** and **8**.

Consider the addition of a proton, the simplest of all electrophiles, to highly substituted 1,2-dihydropyridine **4a** (Fig. 2). The four most likely products are *cis* and *trans* stereoisomers of reactive iminium ions **5a** and **6a**, obtained by protonation at the  $\alpha$  and  $\gamma$  positions, respectively. Each of these reactive intermediates might also be expected to undergo additional transformations to give undesired by-products such as enamine tautomers or dimers and higher-order oligomers.

Despite the large potential number of products, we directed our efforts at the selective formation of single iminium isomers (18, 19). When a strong acid with a  $pK_a$  (where  $K_a$  is the acid dissociation constant) several units below that of **4a** is used,  $\alpha$  protonation occurs under kinetic control to give **5a** as the major product (Fig. 2). Preferred kinetic protonation at the  $\alpha$  position is consistent with electrophilic attack reported for conjugated dienolates (20). A screening of acids and solvents showed that arylsulfonic acids in dichloromethane afford  $\alpha$ -protonated *cis*-**5a** as a single diastereomer with >95% selectivity. Thus, treatment of **4a** with 1.1 equivalents of  $\text{PhSO}_3\text{H}$  in dichloromethane at room temperature resulted in complete protonation within 15 min as evidenced by  $^1\text{H}$  nuclear magnetic resonance (NMR) spectroscopy. Isomerization to other species, eventually *trans*-**6a**, took place with a half life of 38 hours.

Protonation of **4a** under thermodynamic control was achieved using two equivalents of a weaker acid and equilibration over 12 to 16 hours at room temperature. Treatment with  $(\text{PhO})_2\text{PO}_2\text{H}$  in tetrahydrofuran (THF) at room temperature gave  $\gamma$ -protonated *trans*-**6a** with >95% regio- and diastereoselectivity. Solutions of *trans*-**6a** remained unchanged at room temperature over weeks and upon heating to 80°C for 1 day, indicating that the thermodynamically most stable ion had formed. From a practical point of view, benzenesulfonic acid and diphenyl phosphoric acid not only permit the directed formation of **5a** and **6a** but also have the advantage of being easily weighable solids that provide iminium salts that are soluble in organic solvents.

To rigorously define the relative stereochemistry and obtain a better understanding of the conformations of the products of protonation, x-ray structures were obtained for kinetically favored iminium ion *cis*-**5a** and thermodynamically favored iminium ion *trans*-**6a**. Moreover, for kinetic iminium ion *cis*-**5a**, a fast crystallization process (2 hours), rather than the typically preferred slow crystal formation, was necessary to prevent iminium equilibration. The ring in kinetic ion *cis*-**5a** adopts a boatlike conformation with the C3-Me and C6-Et substituents in pseudoaxial positions (Fig. 3A1). The piperidine ring in the thermodynamic ion *trans*-**6a** exhibits a more planar geometry of the N–C1–C2–C3 moiety with the C5-Et and C6-Et substituents now disposed in pseudoaxial positions (Fig. 3A2). Presumably, the pseudoaxial

<sup>1</sup>Department of Chemistry, Yale University, New Haven, CT 06520, USA. <sup>2</sup>Division of Chemical Sciences, Lawrence Berkeley National Laboratory, and Department of Chemistry, University of California, Berkeley, CA 94720, USA.

\*To whom correspondence should be addressed. E-mail: jonathan.ellman@yale.edu

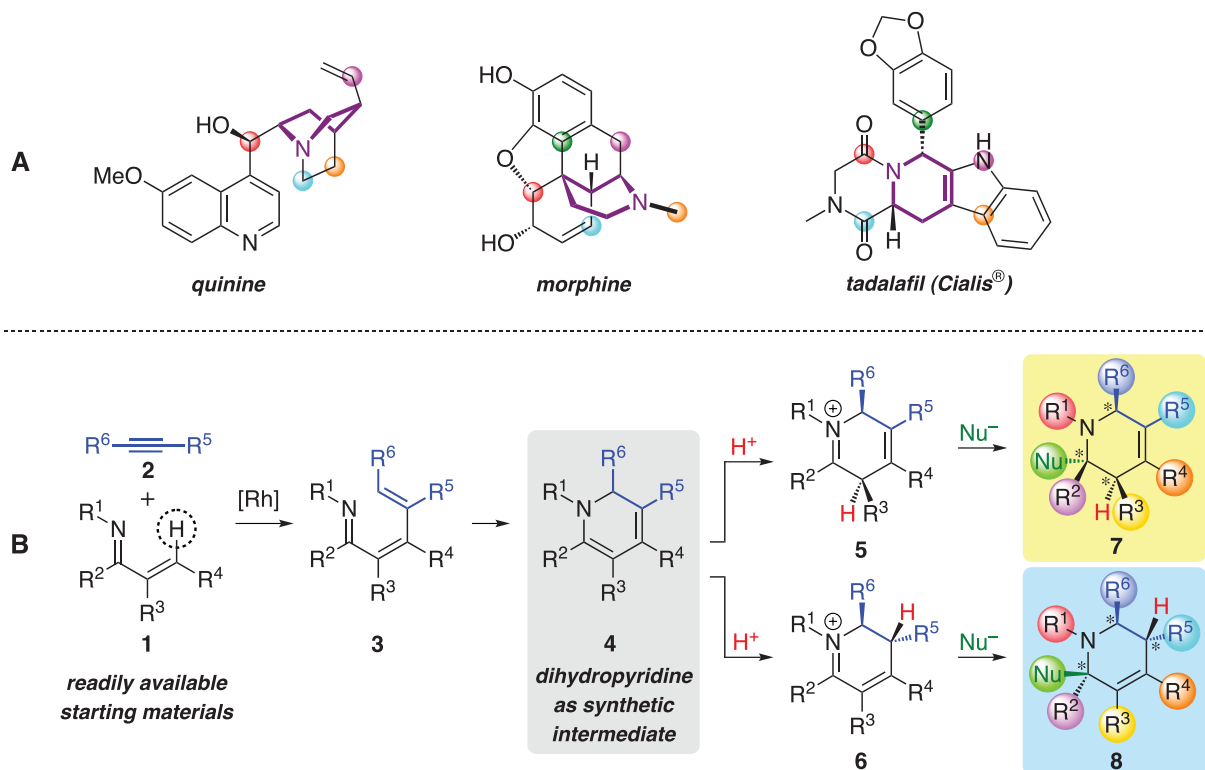


**Fig. 1.** (A) Drugs containing a multiply substituted piperidine core. (B) Rhodium-catalyzed synthesis of dihydropyridine intermediates leading to piperidine derivatives.

orientation of the substituents on the saturated carbons for both the kinetic and thermodynamic iminium ions avoids unfavorable A-1,2-interactions.

Density functional theory (DFT) calculations were carried out at the B3LYP/6-311G+(d,p) level of theory to further characterize the energies and conformations for the four possible protonation products (21). The kinetic iminium ion *cis*-**5a** was calculated to adopt a boatlike conformation with the C3-Me and C6-Et groups in pseudoaxial positions, consistent with the x-ray structure (Fig. 3B1). The alternative boatlike conformation with the C3-Me and C6-Et groups in pseudoequatorial positions was calculated to be higher in energy by 8.3 kcal/mol, consistent with the unfavorable A-1,2-interactions imparted by adjacent alkenyl methyl groups (22). The thermodynamic protonation product *trans*-**6a** was calculated to be the most stable of the four possible iminium ions by >3 kcal/mol, consistent with its being the only observable isomer under thermodynamic control (Fig. 3B2). The overall geometry, bond distances, and angles obtained with the DFT calculations are in very good agreement with the structures obtained for both *cis*-**5a** and *trans*-**6a**.

The conditions developed for kinetic and thermodynamic protonation to provide single diastereomers of reactive iminium ions set the stage for an extremely efficient protocol to prepare distinct regio- and diastereomeric tetrahydropyridines **7** and **8** with multiple stereogenic centers. Dihydropyridines **4** are first prepared by the aforementioned Rh-catalyzed cascade process from commercially available alkynes **2** and imines **1**, which are in turn readily prepared from common enones and primary amines. Kinetic protonation of **4** at the  $\alpha$  position provides iminium ions **5**, which upon nucleophilic addition should provide tetrahydropyridines **7**. Alternatively, thermodynamic protonation at the  $\gamma$  position provides ions **6**, to which nucleophilic addition should provide tetrahydropyridines **8**, respectively. Variation of the substitution pattern in each starting component should result in a vast number of potential permutations in the stable piperidine derivatives **7** and **8**.

We first sought to explore reductions to provide hydride addition products **7** and **8** obtained from kinetic and thermodynamic protonation, respectively (Fig. 4). We recently reported that upon formation of dihydropyridine **4** treatment with Na[(AcO)<sub>3</sub>BH] in the presence of acetic acid provides **7** (Nu = H) in good overall yields based upon starting imine **2** with uniformly very high stereoselectivity (17). This reaction presumably proceeded by in situ formation and then reduction of kinetic iminium **5**.

To explore reduction of the thermodynamically favored iminiums **6**, formation of **6a** under thermodynamic control was followed by reduction with the mild hydride donor [(AcO)<sub>3</sub>BH]<sup>-</sup> in THF to afford tetrahydropyridine **8a** in an 80% overall yield with respect to imine **1a** (Fig. 4, conditions B and C). Compound **8a** was formed as a single diastereomer as evidenced by NMR

spectra of the crude product mixture; its relative configuration of the saturated ring carbon atoms was established unambiguously by x-ray crystallography (fig. S4). Starting from differently substituted imine and alkyne precursors, products **8b-i** were obtained in high overall yields of 61 to 87% (Fig. 4). More importantly, very high diastereoselectivities were observed uniformly except for **8b** and **8g**, which were obtained as a 10:1 and 8.5:1 mixture of two diastereomers, respectively. In the case of **8g**, reduction using Li[*i*-Bu<sub>3</sub>BH] increased the diastereoselectivity to >95% and showed that

improvement of diastereomeric ratio was possible using a sterically more demanding reducing agent. Tolerance of different *N*-substituents (**8a-c**), unsymmetrical and functionalized alkynes (**8d-f**), as well as (hetero-)aryl substituents (**8g-i**) underscored the generality of the methodology.

Through this sequence, the piperidine products **8** were obtained via the direct generation of iminium ions **6** from imine and alkyne inputs. Isolation of the dihydropyridine intermediate **4** before protonation and reduction was only necessary for the preparation of products **8e** and **8f**. All other highly

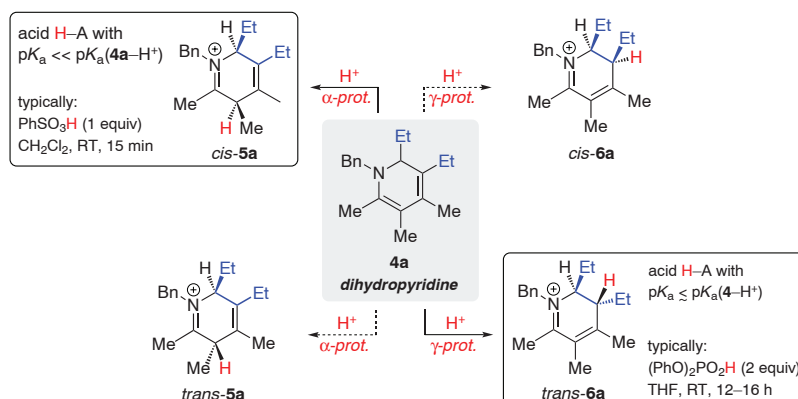


**Fig. 2.** Four possible iminium ions resulting from protonation of dihydropyridine **4a**. RT, room temperature.

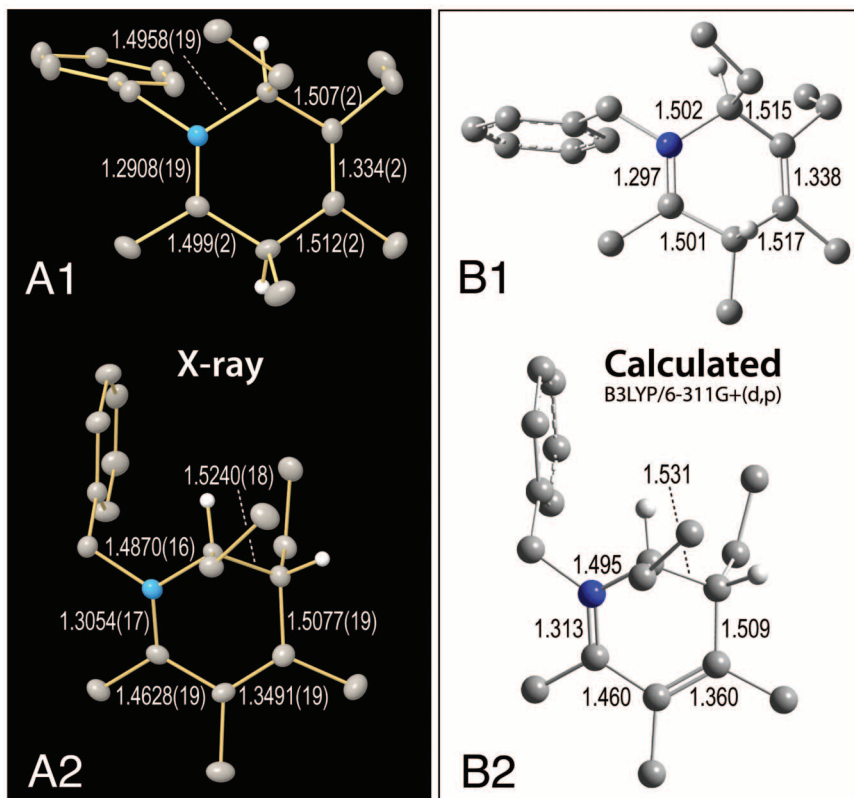


**Fig. 3.** X-ray crystal structures (displayed with 50% displacement ellipsoids) of iminium ions (**A1**) *cis*-**5a** and (**A2**) *trans*-**6a**; calculated structures of (**B1**) *cis*-**5a** and (**B2**) *trans*-**6a**. Numbers are bond lengths in Å; H atoms have been omitted except when attached to saturated ring atoms.

substituted piperidine derivatives required only a single workup and purification at the end of the sequence.

Successful hydride reduction of the iminium ions suggested the feasibility of diastereoselective addition of carbon nucleophiles, although competitive deprotonation pathways posed a challenge. Iminium ions **5** and **6** both exhibited C2-electrophilic C2 positions but also Brønsted-acidic  $\alpha$  and  $\gamma$  sites where protonation of the  $\pi$  system of **4** had oc-

curred. Organometallic reagents R-[M] of high Brønsted basicity, such as alkylolithiums and alkyl Grignard reagents, led to mixtures of C2-addition products **7** or **8** and dihydropyridines **4** resulting from deprotonation. We identified several nucleophiles that underwent clean 1,2-addition and afforded only minor amounts of undesired elimination products. Allyl, benzyl, alkynyl, and ester groups could be introduced using allyl-[CeCl<sub>2</sub>], ArCH<sub>2</sub>-[CeCl<sub>2</sub>], RC≡C-[MgCl], and ROC(O)CH<sub>2</sub>-[ZnBr]

reagents, respectively. Organometallic reagents were selected that favor electrophilic addition over competitive deprotonation pathways (23).

Addition reactions to both *cis*-**5** and *trans*-**6** proceeded in high yields and excellent diastereoselectivities (Fig. 4). For these transformations, the dihydropyridine intermediates **4** were separated from the rhodium catalyst by filtration through alumina, converted to the iminium ions with PhSO<sub>3</sub>H or (PhO)<sub>2</sub>PO<sub>2</sub>H, and added to an excess of the carbon nucleophile in THF or diethyl ether. Tetrahydropyridines **7a–g** and **8j–q** were obtained in yields of 66 to 94% and with diastereoselectivities of 94:6 or higher. NMR spectra of the crude products confirmed that the diastereoselectivities were not a result of selective isolation of one particular stereoisomer. In analogy to the hydride reductions of **6**, exclusive 1,2-addition (no 1,4-derivatization) was observed. Relative configurations were inferred on the basis of crystal structures of **7a** (17), **7e**, and **8m** (figs. S3 and S5) and the similarities of the NMR spectra of the two sets of products. Compounds **7** exhibited all-*cis* stereochemistry of the substituents R<sup>2</sup>, R<sup>3</sup>, and R<sup>6</sup>, whereas for **8** *trans*-R<sup>5</sup>/R<sup>6</sup> and *trans*-R<sup>6</sup>/R<sup>2</sup> stereochemistry was observed. Thus, the facial selectivity for the addition step was the same for [(AcO)<sub>3</sub>BH]<sup>−</sup> and the organometallic reagents, suggesting that the preferred trajectory was mainly determined by the geometry of the iminium ions **5** and **6** and to a lesser extent by the nature of the nucleophile. Tetrahydropyridine **8q** features seven different substituents as a result of coupling of a differentially substituted imine with an unsymmetrical alkyne and addition of an alkynyl nucleophile. Such a level of directed placement of substituents around a piperidine ring has not been reported to the best of our knowledge (21, 22).

The x-ray structures of the reactive iminium ions *cis*-**5a** and *trans*-**6a** offer prospective insight into the high diastereoselectivities that were consistently observed in the nucleophilic addition steps. Nucleophilic addition to ion *cis*-**5a** is most likely directed by the pseudoaxial C3 substituent, which exerts the strongest steric hindrance to nucleophiles approaching the C2 electrophilic center. The relatively planar C2–C3–C4 moiety of *trans*-**6a** provides little facial steric bias for the incoming nucleophile. We therefore hypothesize that the conformation of the benzyl group might govern diastereoselectivity in the addition step.

Although pharmaceutical researchers now routinely and reliably separate enantiomers by preparative chiral high-performance liquid chromatography (24, 25), an asymmetric variant of the present reaction sequence could be contemplated through the use of chiral directing groups or asymmetric electrocyclic catalysts (26, 27). Moreover, the addition of many other types of nucleophiles should be possible, and the 1,2-dihydropyridine intermediates **4** could conceivably react with electrophiles other than protons to enable the regio- and stereoselective synthesis of even more densely substituted products.

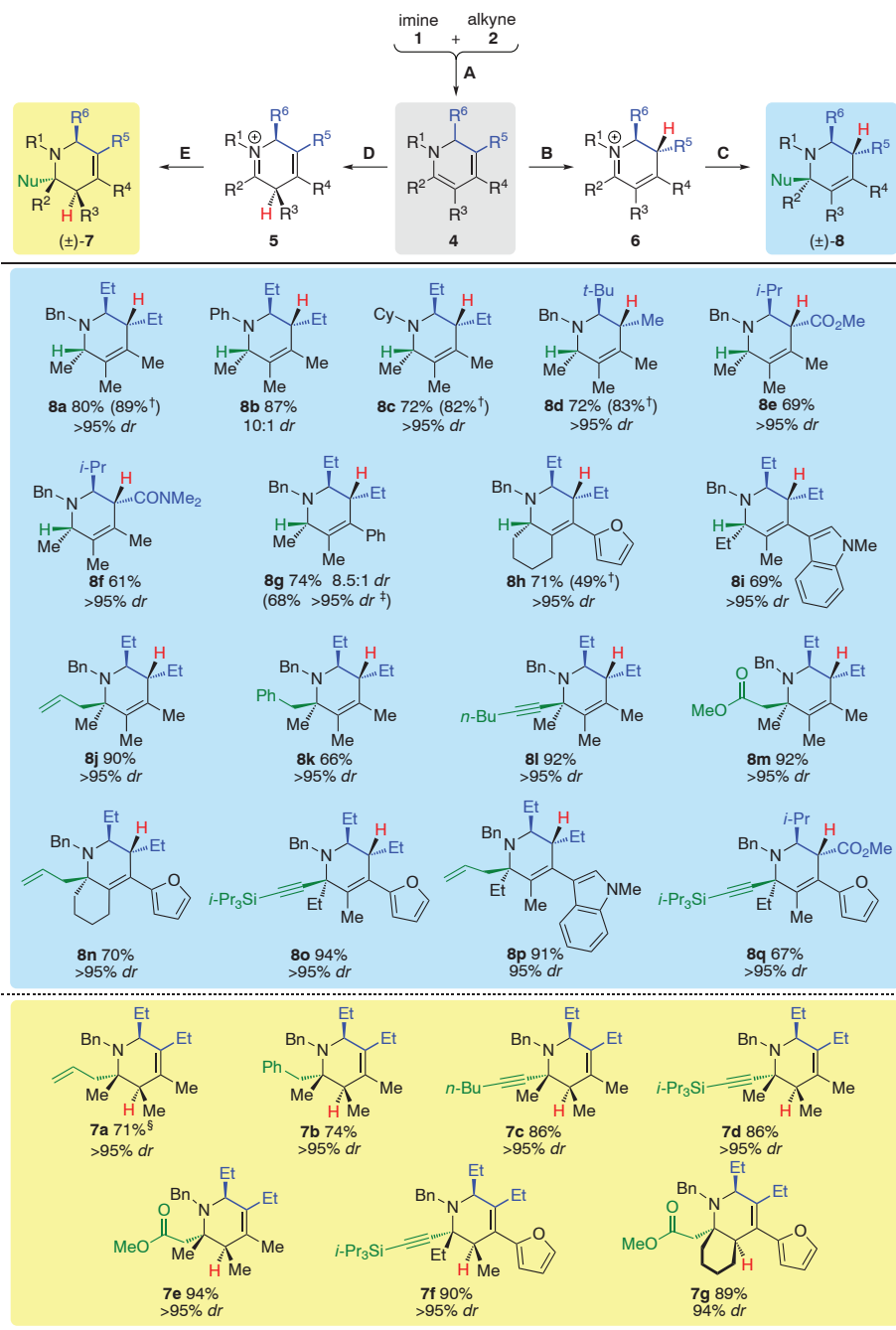


**Fig. 4.** Substrate scope for the synthesis of products **7** and **8**. Conditions: (A) 1:2 [RhCl(cyclooctene)]<sub>2</sub>/4-Me<sub>2</sub>NC<sub>6</sub>H<sub>4</sub>-PET<sub>2</sub> (1 to 2.5 mol %), PhMe. (B) (PhO)<sub>2</sub>PO<sub>2</sub>H, THF. (C) Na[(AcO)<sub>3</sub>BH], THF or R-[M], THF or Et<sub>2</sub>O. (D) PhSO<sub>3</sub>H, CH<sub>2</sub>Cl<sub>2</sub>. (E) R-[M], THF or Et<sub>2</sub>O; for experimental details, see the Supplementary Materials. †[Rh] step run in THF, and reaction carried out as a one-pot procedure; ‡[Rh] step run in THF, and reduction conducted using Li[*i*-Bu<sub>3</sub>BH]; §(17).

## References and Notes

- Typing the name of these drug and drug candidates into PubChem (<http://pubchem.ncbi.nlm.nih.gov/>) provides the compound structure, bioactivity, full list of published studies, and information regarding ongoing clinical trials, applications, and usage: plavix (CID 60606), cialis (110635), and aricept (CID 5741).
- F. Lovering, J. Bikker, C. Humblet, *J. Med. Chem.* **52**, 6752 (2009).
- W. P. Walters, J. Green, J. R. Weiss, M. A. Murcko, *J. Med. Chem.* **54**, 6405 (2011).
- T. J. Ritchie, S. J. F. Macdonald, *Drug Discov. Today* **14**, 1011 (2009).
- M. P. Doyle, K. I. Goldberg, *Acc. Chem. Res.* **45**, 777 (2012).
- H. M. L. Davies, J. Du Bois, J.-Q. Yu, *Chem. Soc. Rev.* **40**, 1855 (2011).
- R. H. Crabtree, *Chem. Rev.* **110**, 575 (2010).
- J. Yamaguchi, A. D. Yamaguchi, K. Itami, *Angew. Chem. Int. Ed.* **51**, 8690 (2012).
- H. M. L. Davies, J. R. Manning, *Nature* **451**, 417 (2008).
- M. Wasa, K. M. Engle, J.-Q. Yu, *J. Am. Chem. Soc.* **132**, 3680 (2010).
- N. Guimond, S. I. Gorelsky, K. Fagnou, *J. Am. Chem. Soc.* **133**, 6449 (2011).
- D. A. Colby, R. G. Bergman, J. A. Ellman, *J. Am. Chem. Soc.* **130**, 3645 (2008).
- L. F. Tietze, G. Brasche, K. Gericke, *Domino Reactions in Organic Synthesis* (Wiley, Weinheim, Germany, 2006).
- H. M. Davies, E. M. Sorensen, *Chem. Soc. Rev.* **38**, 2981 (2009).
- C. Grondal, M. Jeanty, D. Enders, *Nat. Chem.* **2**, 167 (2010).
- J. A. Bull, J. J. Mousseau, G. Pelletier, A. B. Charette, *Chem. Rev.* **112**, 2642 (2012).
- S. Duttwyler, C. Lu, A. L. Rheingold, R. G. Bergman, J. A. Ellman, *J. Am. Chem. Soc.* **134**, 4064 (2012).
- R. E. Lyle, D. A. Nelson, P. S. Anderson, *Tetrahedron Lett.* **3**, 553 (1962).
- P. S. Anderson, R. E. Lyle, *Tetrahedron Lett.* **5**, 153 (1964).
- D. A. Evans, in *Asymmetric Synthesis*, Vol. 3 (Academic Press, New York, 1984), pp. 20–21 and 65–68.
- M. J. Frisch *et al.*, Gaussian 09, Revision A.1 (Gaussian, Inc., Wallingford, CT, 2009).
- R. W. Hoffmann, *Chem. Rev.* **89**, 1841 (1989).
- H.-J. Liu, K.-S. Shia, X. Shang, B.-Y. Zhu, *Tetrahedron* **55**, 3803 (1999).
- T. J. Ward, K. D. Ward, *Anal. Chem.* **82**, 4712 (2010).
- Y. Okamoto, T. Ikai, *Chem. Soc. Rev.* **37**, 2593 (2008).
- S. Thompson, A. G. Coyne, P. C. Knipe, M. D. Smith, *Chem. Soc. Rev.* **40**, 4217 (2011).
- S. Müller, B. List, *Angew. Chem. Int. Ed.* **48**, 9975 (2009).

**Acknowledgments:** This work was supported by NIH grant GM069559 (to J.A.E.). R.G.B. acknowledges funding from the Director, Office of Energy Research, Office of Basic Energy Sciences, Chemical Sciences Division, U.S. Department of Energy, under contract DE-AC02-05CH11231. S.D. is grateful to the Swiss National Science Foundation for a postdoctoral fellowship (PBZHP2-130-966). Metrical parameters for the structures of compounds 5a, 6a, 7e, 8a, and 8m are available free of charge from the Cambridge Crystallographic Data Centre under reference nos. CCDC 911314–911318.

**Supplementary Materials**

[www.sciencemag.org/cgi/content/full/339/6120/678/DC1](http://www.sciencemag.org/cgi/content/full/339/6120/678/DC1)  
Materials and Methods  
Figs. S1 to S5  
Tables S1 to S7  
References (28–35)

25 September 2012; accepted 3 December 2012  
10.1126/science.1230704

# A Functional [NiFe]Hydrogenase Mimic That Catalyzes Electron and Hydride Transfer from H<sub>2</sub>

Seiji Ogo,<sup>1,2,3\*</sup> Koji Ichikawa,<sup>2</sup> Takahiro Kishima,<sup>2</sup> Takahiro Matsumoto,<sup>1,2</sup> Hidetaka Nakai,<sup>1,2</sup> Katsuhiko Kusaka,<sup>4</sup> Takashi Ohhara<sup>5</sup>

Chemists have long sought to mimic enzymatic hydrogen activation with structurally simpler compounds. Here, we report a functional [NiFe]-based model of [NiFe]hydrogenase enzymes. This complex heterolytically activates hydrogen to form a hydride complex that is capable of reducing substrates by either hydride ion or electron transfer. Structural investigations were performed by a range of techniques, including x-ray diffraction and neutron scattering, resulting in crystal structures and the finding that the hydrido ligand is predominantly associated with the Fe center. The ligand's hydridic character is manifested in its reactivity with strong acid to liberate H<sub>2</sub>.

Nickel-iron hydrogenase enzymes ([NiFe]H<sub>2</sub>ases) catalyze the transfer of electrons from hydrogen gas (H<sub>2</sub>) to a redox partner (1–5). This activation of H<sub>2</sub> for the release of electrons and/or hydride ions has tremendous potential applications from energy generation to industrial synthesis, and so H<sub>2</sub>ases

are currently the focus of much research across many disciplines.

We have previously reported a [NiRu]model complex ([Ni<sup>II</sup>(X)(H<sub>2</sub>O)(μ-H)Ru<sup>II</sup>(C<sub>6</sub>Me<sub>6</sub>)(NO<sub>3</sub>)<sub>3</sub>]{[3](NO<sub>3</sub>), where X = N,N'-dimethyl-3,7-diazanonane-1,9-dithiolato and Me indicates a methyl group}) that can mimic the chemical functions of [NiFe]H<sub>2</sub>ases (6, 7). Based on the [NiRu] core, this complex could activate H<sub>2</sub> in water, at room temperature, and use the extracted electrons to reduce substrates as part of a catalytic cycle. A central finding of this study was that the so-called hydride complex actually took the form of a three-center Ni–H–Ru bond—in other words, the electrons from the hydride were used to form a Ni<sup>I</sup>–Ru<sup>I</sup> bond with the proton. Because no functional hydride-type model had been reported, we were confident that the protic form was the best descriptor of the active state of [NiFe]H<sub>2</sub>ases.

As a result of our efforts to improve this original model, we can now report a functional model complex based on a [NiFe] core. Furthermore, this complex bears a true hydride ion in the reactive form. Not only is this catalyst far

cheaper than our previous complex, it constitutes a major step forward in the understanding of [NiFe]H<sub>2</sub>ases. Here, we describe the synthesis of this model and report its chemical and structural features.

Model complex ([Ni<sup>II</sup>(X')Fe<sup>II</sup>(MeCN){P(OEt)<sub>3</sub>}]<sub>3</sub>(BPh<sub>4</sub>)<sub>2</sub> {[1](BPh<sub>4</sub>)<sub>2</sub>, where X' = N,N'-diethyl-3,7-diazanonane-1,9-dithiolato, Et indicates an ethyl group, and Ph a phenyl group}) bears the characteristics that we have previously described as necessary for a [NiFe]H<sub>2</sub>ase model complex: a bimetallic core, a μ-S bridge between the metal centers to allow close approach, and ligands capable of accepting π-back donation from the Fe (or Ru) center. The three most important developments in this complex are the replacement of Ru with Fe, the replacement of an aryl ligand with three triethylphosphite {P(OEt)<sub>3</sub>} ligands, and, crucially, the use of sodium methoxide (MeONa) as a base instead of water.

The structure of **1**, bearing a MeCN ligand at the vacant site, was determined by x-ray diffraction (fig. S1), proton nuclear magnetic resonance (<sup>1</sup>H NMR) spectroscopy (fig. S2), and mass spectrometry (fig. S3) (8). The Ni···Fe distance is 3.3189(6) Å. The Ni–S–Fe angles are 94.93(4) and 94.79(4)°.

Complex **1** heterolytically activated H<sub>2</sub> in MeCN/MeOH at room temperature and atmospheric pressure. Abstraction of a proton from bound H<sub>2</sub> by a strong base (MeONa) resulted in formation of hydride-bearing complex ([Ni<sup>II</sup>(X')(μ-H)Fe<sup>II</sup>{P(OEt)<sub>3</sub>}]<sub>3</sub>(BPh<sub>4</sub>)<sub>2</sub> {[2](BPh<sub>4</sub>)<sub>2</sub>}) (8).

The structure of the hydride-bearing complex **2** was determined by x-ray diffraction (Fig. 1), neutron scattering (fig. S4), <sup>1</sup>H NMR (fig. S5) and infrared (IR) spectroscopy (fig. S6), and mass spectrometry (fig. S7). The Ni atom adopts the same planar structure as in **1**, and the Ni···Fe distance is 2.7930(6) Å, which is also comparable to the Ni···Ru distance in **3**. These distances are, however, longer than the Ni···Fe separation in

<sup>1</sup>World Premier International Research Center Initiative–International Institute for Carbon-Neutral Energy Research (WPI-I2CNER), Kyushu University, 744 Moto-oka, Nishi-ku, Fukuoka 819-0395, Japan. <sup>2</sup>Department of Chemistry and Biochemistry, Graduate School of Engineering, Kyushu University, 744 Moto-oka, Nishi-ku, Fukuoka 819-0395, Japan. <sup>3</sup>Core Research for Evolutional Science and Technology (CREST), Japan Science and Technology Agency (JST), Kawaguchi Center Building, 4-1-8 Honcho, Kawaguchi, Saitama 332-0012, Japan. <sup>4</sup>Frontier Research Center for Applied Atomic Sciences, Ibaraki University, IBARAKI Quantum Beam Research Center (IQBRC) Building, 162-1 Shirakata, Tokai, Ibaraki 319-1106, Japan. <sup>5</sup>Research Center for Neutron Science and Technology, Comprehensive Research Organization for Science and Society, IQBRC Building, 162-1 Shirakata, Tokai, Ibaraki 319-1106, Japan.

\*To whom correspondence should be addressed. E-mail: ogotcm@mail.cstm.kyushu-u.ac.jp